Observation of Dirac cone band dispersions in FeSe thin films by photoemission spectroscopy

S. Y. Tan,[1] Y. Fang,[1] D. H. Xie,[1] W. Feng,[1] C. H. P. Wen,[2] Q. Song,[2] Q. Y. Chen,[1,2] W. Zhang,[1] Y. Zhang,[1] L. Z. Luo,[1] B. P. Xie,[2] X. C. Lai,[1,*] and D. L. Feng[2,†]

[1]*Science and Technology on Surface Physics and Chemistry Laboratory, Mianyang 621908, China*

[2]*Physics Department, Applied Surface Physics State Key Laboratory, and Advanced Materials Laboratory, Fudan University, Shanghai 200433, China*

(Received 13 December 2015; revised manuscript received 24 January 2016; published 9 March 2016)

The search for novel materials with Dirac cone band dispersion is one of the most challenging and important works for both fundamental physics and technological applications. Here, we studied the electronic structure of FeSe thin films grown on $SrTiO_3$ substrates by angle-resolved photoemission spectroscopy (ARPES). We revealed the existence of Dirac cone band dispersions in FeSe thin films thicker than 1 unit cell below the nematic transition temperature, whose apexes are located −10 meV below Fermi energy. The evolution of electronic structures for FeSe thin films as a function of temperature, thickness, and cobalt doping were systematically studied. The Dirac cones coexist with the nematicity in FeSe and disappear when nematicity is suppressed. Our results provide useful guidelines for understanding the novel electronic structure, nematicity, and superconductivity in the FeSe system.

DOI: 10.1103/PhysRevB.93.104513

I. INTRODUCTION

The discovery of high temperature superconductivity in single unit cell (UC) FeSe film grown on $SrTiO_3$ (STO) substrate has attracted extensively attention [1–9]. A superconducting gap as large as 20 meV was first discovered [1] by scanning tunneling spectroscopy (STS), which was later confirmed [2–4] by angle-resolved photoemission spectroscopy (ARPES) measurements. Then, the T_C above 40 and 100 K in 1 UC FeSe films has been demonstrated by direct transport measurements [8] and *in situ* electrical transport measurements [9], respectively. Until now, the superconducting mechanism for single layer FeSe is still unsolved. Another hotly debated issue is the driving force of the nematicity for FeSe. Bulk FeSe undergoes a tetragonal to orthorhombic transition at $T_s \sim 90$ K, and at $T_c \sim 8$ K superconductivity sets in [10]. Clear band splitting around the Brillouin zone corner was first discovered in multilayer FeSe thin films [4], with a characteristic temperature much higher than the structure transition temperature (T_s), which is thought to be caused by short ranged magnetic order. Then similar band reconstruction was also found in bulk FeSe single crystals [11], which was interpreted to be triggered by the electronic nematicity. Although the existence of nematic order in FeSe is by now a well-established experimental fact, its origin remains controversial. Spin, orbital degrees of freedom, or their complicated coupling are all possible candidates of the driving force as proposed by many researchers [12–23].

Another intriguing issue in modern condensed matter physics is the massless Dirac fermion states in materials, such as graphene [24], topological insulators [25,26], Weyl semimetals [27,28], as well as the parent compound of iron-based superconductors [29–32]. Dirac cone states have been theoretically predicted [29] and experimentally confirmed [30–32] in $BaFe_2As_2$ below the spin density wave (SDW) transition temperature. It is well established that the formation of Dirac cone states is a consequence of the nodes of the SDW gap by complex zone folding in bands with different parities. Surprisingly, ultrafast Dirac conelike carriers were found in FeSe single crystals by electric transport measurement [33], although no static magnetic order exists in FeSe. Furthermore, a recent density functional theory (DFT) calculation [34] predicted a magnetic order named the "pair-checkerboard AFM" as the magnetic ground state of tetragonal FeSe, which can also induce Dirac cone band dispersion in FeSe. Thus, it is important to study the possible Dirac cone states and the related nematicity in FeSe.

In this paper, we report an ARPES investigation of the low-energy electronic states of FeSe thin films grown on STO substrates. We revealed the existence of Dirac cone band dispersions in FeSe thin films thicker than 1 UC below the nematic transition temperature. The Dirac cones sit at the small spots of high photoemission intensity on the Fermi surface, whose apexes are located −10 meV below Fermi energy (E_F), leading to small electron Fermi pockets. The Dirac cone band structures disappear above the nematic transition temperature and barely change as a function of film thickness. Upon cobalt doping in multilayer FeSe films, the nematicity is suppressed significantly and the Dirac cones disappear simultaneously.

II. EXPERIMENT

High-quality FeSe single crystalline thin films were grown on the TiO_2 terminated and Nb-doped STO (0.5 wt%) substrate with the molecular beam epitaxy (MBE) method following the previous reports [1,4]. After growth, the film was directly transferred from the MBE chamber into the ARPES chamber with typical vacuum of 5×10^{-11} mbar. The electron doping is induced by depositing cobalt atoms on the surface of as grown FeSe thin film and a subsequent 3 h of 600 °C annealing process. ARPES was conducted with 21.2 eV photons from a helium discharge lamp. A Scienta R4000 analyzer was used to record ARPES spectra with typical energy and angular resolutions of 10 meV and 0.2°, respectively. A freshly

*laixinchun@caep.cn

†dlfeng@fudan.edu.cn

evaporated gold sample in electrical contact with the FeSe sample served to calibrate E_F.

III. RESULTS AND DISCUSSIONS

The electronic structure of 50 UC FeSe thin film at 30 K is presented in Fig. 1. The photoemission intensity map is integrated over a [E_F −10 meV, E_F + 10 meV] window around the Fermi energy (E_F) as shown in Fig. 1(a). The observed Fermi surface consists of crosslike electron pockets centered at M and elliptical hole pockets centered at Γ. The band structure along the Γ-M direction is shown in Fig. 1(b). From the second derivative of the intensity plot with respect to energy in Fig. 1(b2), one can clearly observe two holelike bands contributing to the elliptical hole pockets at Γ, where one band crosses E_F and the other one has its band top touching E_F. The electronic structure around M is much more complicated and mainly consists of two electronlike bands and two holelike bands, which form the cross shaped electron pockets.

The Fermi surface topology of 50 UC FeSe at 30 K is very similar to those observed in $BaFe_2As_2$ [35] and NaFeAs [36] in their SDW states. Dirac cone band dispersions are discovered at the two very bright spots with high photoemission intensity on the Fermi surface of $BaFe_2As_2$ [31] along the kx direction (Γ-M direction). There are also two bright spots on the Fermi surface of 50 UC FeSe film along kx direction (Γ-M direction). The low-energy electronic structure at 80 K at the brightest spot (labeled as Λ′) is present in Fig. 1(c1), which clearly shows a Λ-like band dispersion near E_F. A distinct Dirac conelike band dispersion can be resolved in Fig. 1(c2), when Fig. 1(c1) is divided by the Fermi-Dirac function convoluted with the instrument resolution function. The main features of Λ′ point are a holelike band (labeled as η) and a Dirac conelike band (labeled as χ). The χ band shows clear X-shaped linear dispersion, which shall form a Dirac cone in three dimensional Brillouin zone. The Dirac point (E_D) is located about −10 meV below E_F, forming a small electron pocket which is responsible for the bright spot on the Fermi surface. The momentum distribution curves (MDCs) near the Dirac cone are present

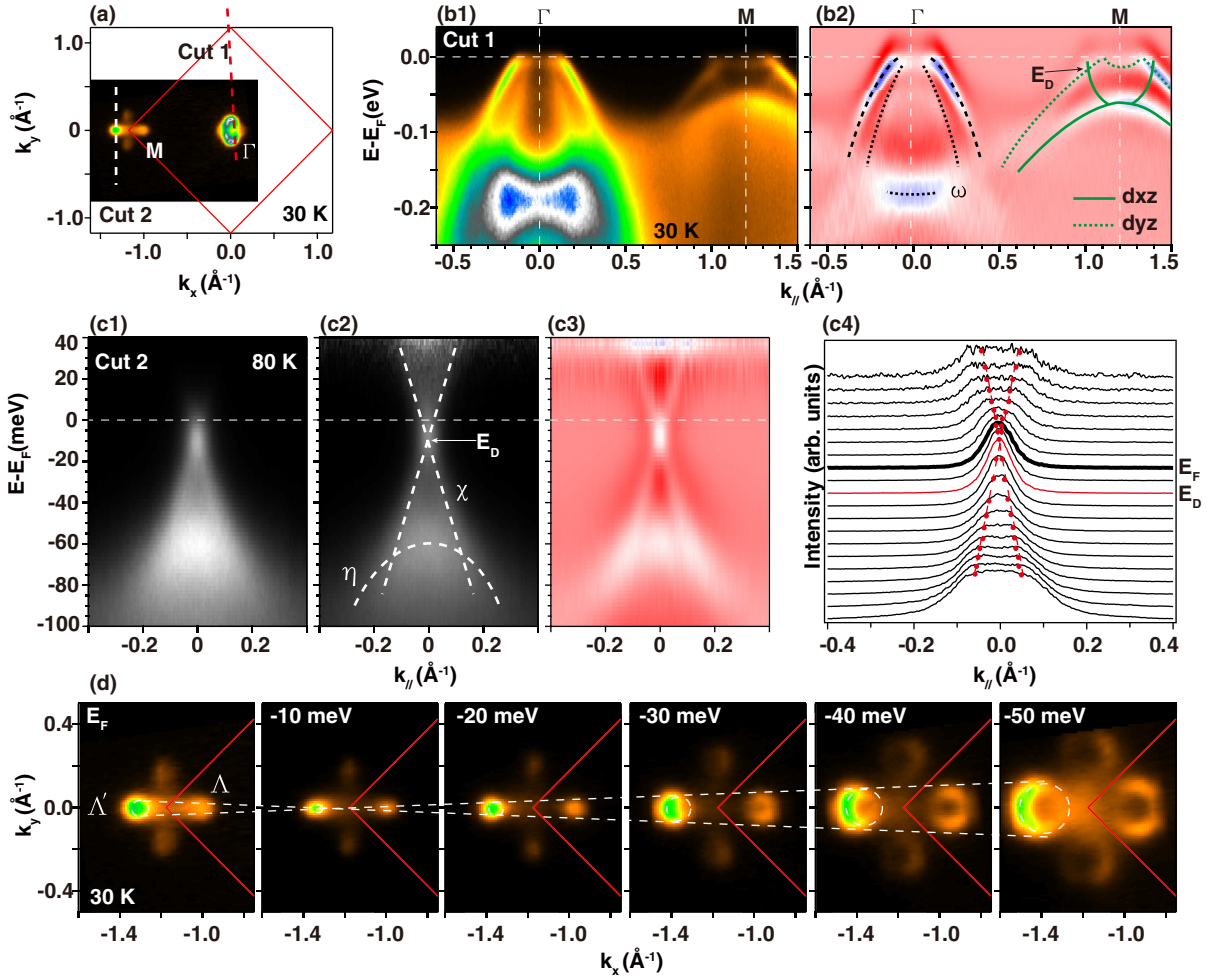

FIG. 1. The Dirac cone band dispersions in 50 UC FeSe thin film. (a) Photoemission intensity map at E_F integrated over [E_F − 10 meV, E_F + 10 meV] at 30 K. (b1) and (b2) The photoemission intensity and its second derivative of the intensity plot with respect to energy along Γ-M direction (cut 1) at 30 K. (c1) The photoemission intensity along cut 2 (cross the brightest spot in the map) at 80 K. (c2) The ARPES spectra (c1) is divided by the Fermi-Dirac function convoluted with the instrument resolution function; the dashed lines are guides to the eye. (c3) The corresponding second derivative of the intensity plot in panel (c2). (c4) The MDCs around the Dirac cone band; the bold black line refers to E_F, and the red line refers to E_D. (d) Constant-energy maps at different binding energies from E_F to E_F − 50 meV.

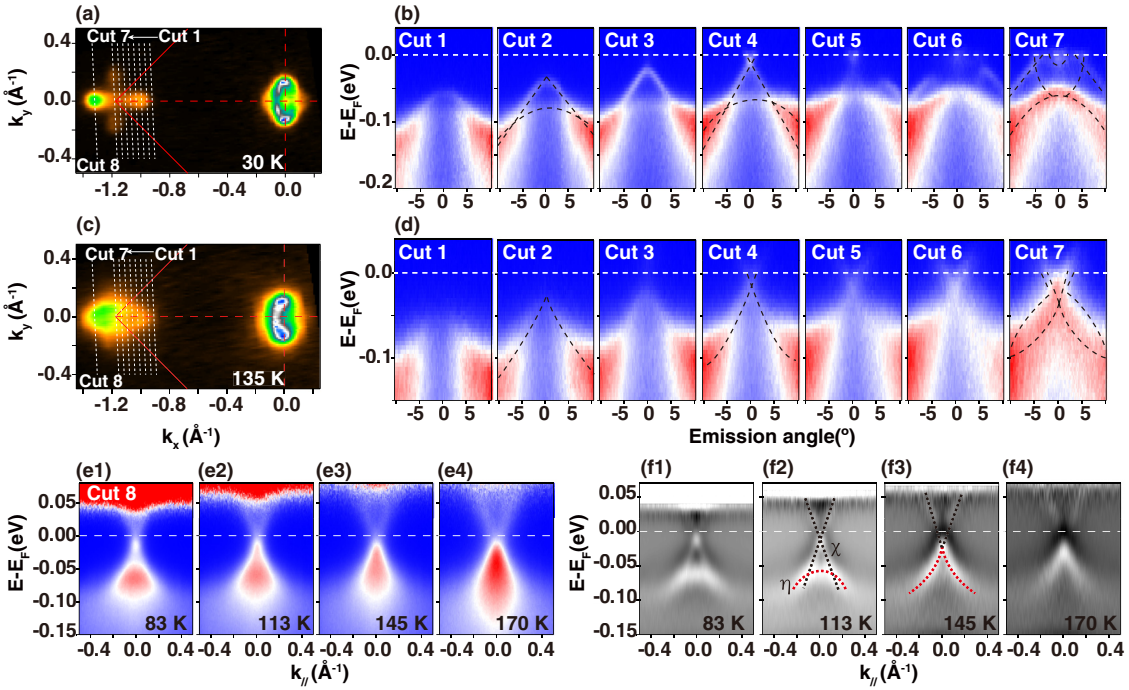

FIG. 2. Temperature dependence of the band structure for 50 UC FeSe thin film. (a) Photoemission intensity map at E_F integrated over $[E_F - 10\ \text{meV}, E_F + 10\ \text{meV}]$ at 30 K. (b) The band structure evolution near M region from cut 1 to cut 7 in (a). (c) Photoemission intensity map at E_F integrated over $[E_F - 10\ \text{meV}, E_F + 10\ \text{meV}]$ at 135 K. (d) The band structure evolution near M region from cut 1 to cut 7 in (c). (e1)–(e4) Temperature dependence of the band structure at Λ' point after division by the Fermi-Dirac function. (f1)–(f4) The corresponding second derivative of the intensity plots of (e1)–(e4).

in Fig. 1(c4); the peaks in the MDCs highlight the position of the χ band. It has been demonstrated that the spin-orbit coupling (SOC) may play an important role in determining the electronic structure of iron-based superconductors [37], which can introduce additional gap at the Dirac point. Limited by the resolution of the ARPES measurement, we cannot completely exclude the existence of gap at the Dirac point. However, from Figs. 1(c2) and 1(c3), we can see that the gap size would be much smaller than 10 meV if it really exists, which is not consistent with the SOC induced band splitting in bulk FeSe (of the order of 20–30 meV) [20]. To further illustrate the cone structure, we present the constant-energy maps at different binding energies from E_F to $E_F - 50$ meV in Fig. 1(d). Four distinct circular Fermi pockets can be resolved around M at the energy $E_F - 50$ meV. The sizes of the circular Fermi pockets gradually decrease when binding energy approaching E_F, reach their minimum at $E_F - 10$ meV (E_D) and then begin to increase. It is a bit confusing that the ARPES measured Fermi surface of FeSe films always maintain the C4 symmetry in the nematic state. According to the STM results [38], the FeSe thin films grown on STO substrate always have structural twin domains that are 90° rotated across the domain boundaries. The four circular Fermi pockets around M point (two Dirac pockets appear on the kx axis and two on the ky axis) may originate from two domains that are 90° rotated with each other. Our data provide direct spectrum evidence that a pair of Dirac cones do exist in FeSe thin films around the Brillouin zone corner, which implies that Dirac fermion states not only exist in iron pnictides but also in iron chalcogenides.

The Fermi surface topologies and band structures around Γ and M are found to get reconstructed across the nematic transition for both thin film and bulk single crystal FeSe samples. One immediate question is whether the Dirac cone band dispersions change across the nematic transition. The Fermi surface and band structure below and above the nematic transition temperature ($T_{nem} = 125$ K) for 50 UC FeSe are presented in Fig. 2. The Fermi surface topology at the M point changes dramatically from cross shaped (30 K) to ellipse shaped (135 K) across the nematic transition, while that around Γ point does not change much. We present a series of cuts [from cut 1 to cut 7 in Fig. 2(a) around M] at 30 K to illustrate the electronic structure reconstruction more clearly in Fig. 2(b). The spectrums taken at the same angles at 135 K are drastically different [Fig. 2(d)], where cuts 4 and 7 correspond to Λ and M points.

The band structure evolution at Λ' point (cut 8) as a function of temperature is shown in Fig. 2(e) after division by the Fermi-Dirac function. Distinct band structure reconstruction can be resolved in the corresponding second derivative of the intensity plots in Fig. 2(f). Below the nematic transition temperature at 113 and 83 K, the main feature at Λ' point is a holelike band η and a Dirac conelike band χ, as illustrated in Fig. 2(f2). At 145 and 170 K above the nematic transition temperature, it seems to be an electronlike band and a holelike band intersect around E_F. The X-like band dispersion that exists in the nematic state disappears above the nematic transition temperature, and it evolves into a conventional electronlike band that crosses E_F to form a slightly larger electron Fermi pocket. Recently, an electric transport measurement under magnetic

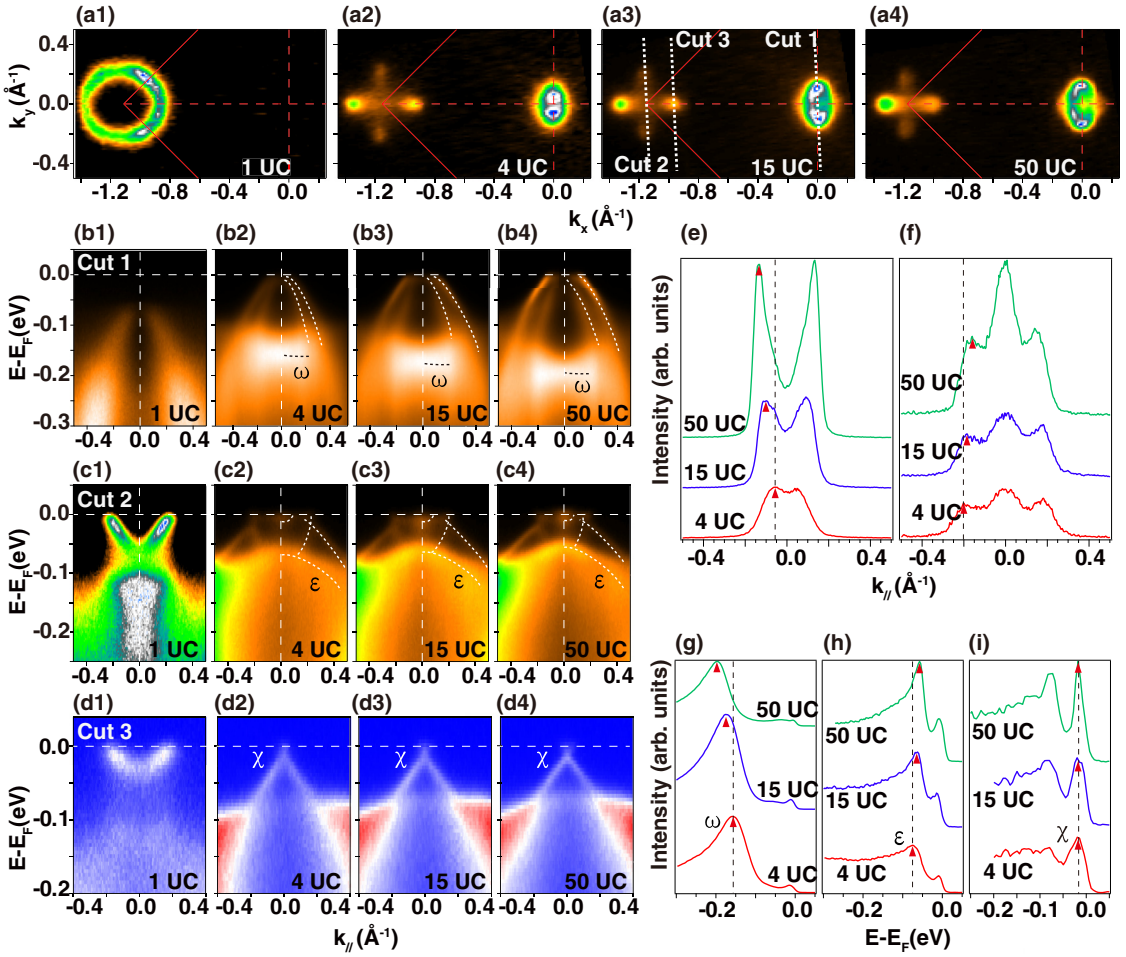

FIG. 3. Thickness dependence of the band structure for FeSe thin films at 30 K. (a) Thickness dependence of the photoemission intensity map at E_F integrated over $[E_F - 10$ meV, $E_F + 10$ meV$]$. (b)–(d) Thickness dependence of the band structure around Γ (b1)–(b4) [cut 1 in (a3)], M (c1)–(c4) [cut 2 in (a3)], and Λ (d1)–(d4) [(cut 3 in (a3)], respectively. (e) and (f) Thickness dependence of the MDCs at E_F around Γ and M, respectively. (g)–(i) Thickness dependence of the EDCs at $k = 0$ around Γ, M, and Λ, respectively.

fields reported possible Dirac conelike ultrafast electrons in FeSe single crystals [33]. By employing *ab initio* mobility spectrum analysis, a remarkable reduction in carrier number and an enhancement in carrier mobility were simultaneously observed below 120 K higher than the structural transition temperature ($T_s = 90$ K) of FeSe single crystal. The previous transport results can be well explained by our ARPES data. Above the nematic transition temperature ($T_{nem} = 125$ K for 50 UC FeSe), a conventional electronlike band with a larger Fermi pocket exist at the Λ′ point. Below the nematic transition temperature, the electronlike band becomes a Dirac conelike band with a smaller Fermi pocket (reduction in carrier number) and ultrafast carrier mobility (enhancement in carrier mobility). Based on the transport and ARPES experimental results, one may conclude that the Dirac cone band dispersions are directly related to the nematicity in FeSe.

The nematic transition temperature has been found to decrease with increasing film thickness in multilayer FeSe films [4], which are 165, 145, and 125 K, respectively for 4, 15, and 50 UC FeSe films. We present thickness dependence of the electronic structure for FeSe thin films at 30 K in Fig. 3 to track the evolution of the Dirac cone band dispersions. The superconducting 1 UC FeSe film ($T_c \sim 50$ K) consists of only electron Fermi pocket at M point [Fig. 3(a1)], which shows no Dirac conelike band at Λ point [Fig. 3(d1)]. The Fermi surface topologies of FeSe films thicker than 2 UC are very much alike [Figs. 3(a2)–3(a4)], while the low-energy bands at Γ and M points change slightly with increased thickness. The spectral weight at Γ point is contributed by two holelike bands for multilayer FeSe films [Figs. 3(b2)-3(b4)]. Their band tops touch E_F in 4 UC film and move upwards with increased thickness, and the hole pockets area increase slightly. The MDCs around E_F at Γ point are shown in Fig. 3(e), in which the peaks represent the Fermi crossing (k_F) of the hole band. One can find that the Fermi crossing becomes larger with increased thickness. Moreover, a nearly flat band named ω moves downwards with increased thickness, which is highlighted by the peaks of the energy distribution curves (EDC) at Γ point in Fig. 3(g).

The band structure near M includes four small electron pockets that make the cross shape. The Fermi crossing of the electron bands become smaller with increased thickness, which are highlighted by the peaks of the MDCs around E_F at M in Fig. 3(f). Moreover, the top of a holelike band labeled ε

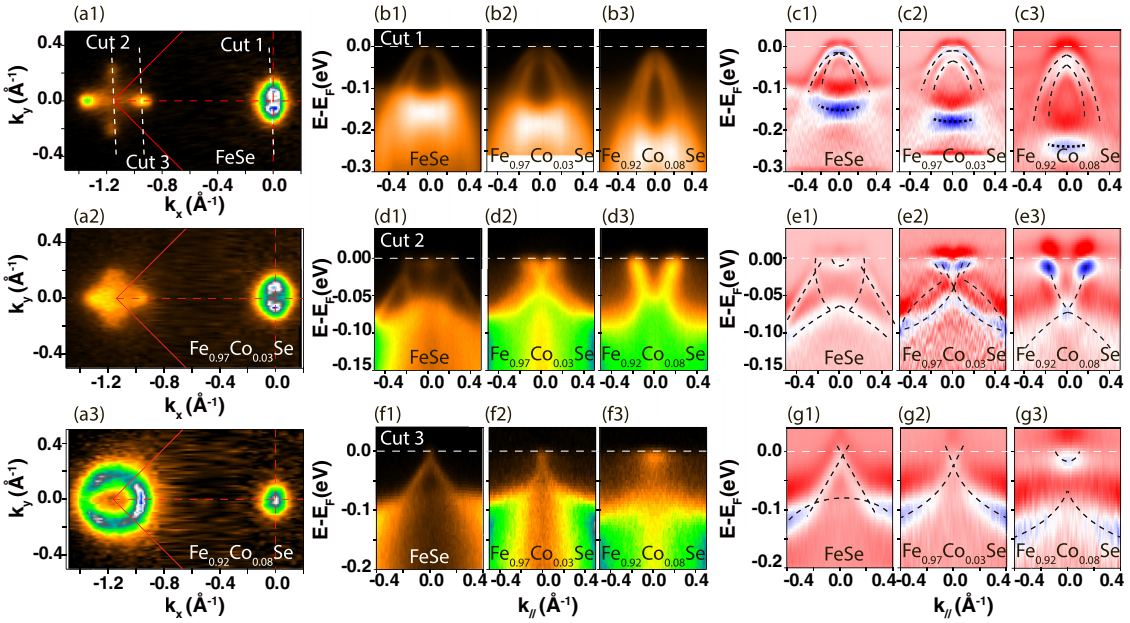

FIG. 4. Doping dependence of the band structure for 4 UC FeSe thin films. (a) Doping dependence of the photoemission intensity map at E_F integrated over [$E_F - 10$ meV, $E_F + 10$ meV]. (b) and (c) Doping dependence of the photoemission intensity (b1)–(b3) and its corresponding second derivative of the intensity plot (c1)–(c3) around Γ [cut 1 in (a1)]. (d) and (e) Doping dependence of the photoemission intensity (d1)–(d3) and its corresponding second derivative of the intensity plot (e1)–(e3) around M [cut 2 in (a1)]. (f) and (g) Doping dependence of the photoemission intensity (f1) and (f3) and its corresponding second derivative of the intensity plot (g1)–(g3) around Λ point [cut 3 in (a1)].

moves upwards with increased thickness, which is highlighted by the peaks of the EDCs at M point in Fig. 3(h). In contrast to the distinct band shifts at Γ and M points, the Dirac cone band dispersion at Λ point barely changes as shown in Fig. 3(d). The EDCs at $k_F = 0$ around Λ point are shown in Fig. 3(i), in which the peaks near E_F represent the position of the Dirac point. The Dirac point shows no obvious change with increasing film thickness within the resolution. In contrast to the SDW state found in $BaFe_2As_2$, the nematicity for FeSe is considered to be originated from the lifting of the orbital degeneracy of d_{xz}/d_{yz} bands, which can cause band crossing to form the observed two Dirac cones around M [Fig. 1(b2)]. Unexpectedly, the Dirac point stays at a fixed energy, while the two bands that form the cones shift with increased film thickness (or decreased nematic order strength).

Theoretically, it has been predicted that nonmagnetic impurities do not affect the Dirac-cone states. Previous studies on the Nernst effect in $Eu(Fe_{1-x}Co_xAs)_2$ [39] and magnetotransport in $Ba(Fe_{1-x}TM_xAs)_2$ (TM = Co, Ni, Cu) [40] indicate that the influence of the Dirac fermion on electronic transport is greatly suppressed by substitution with other 3d transition metals. We used cobalt as dopant and measured the doping dependence of the electronic structure for 4 UC FeSe films, which is shown in Fig. 4. The Fermi surface topology of 4 UC FeSe changes dramatically upon cobalt doping. With about 3% cobalt doping, the cross shaped electron pockets around M in undoped films [Fig. 4(a1)] change to two intersecting elliptical pockets [Fig. 4(a2)], which agrees well with the theoretic predicated Fermi surface of ion based superconductor in the paramagnetic state [41]. When the cobalt doping level increased to 8%, a nearly circular electron Fermi pocket emerges at M [Fig. 4(a3)], which is similar to the Fermi surface of 1 UC FeSe [Fig. 3(a1)]. This is in contrast to the potassium-doped multilayer FeSe thin films, where superconductivity up to 40 K was observed by both ARPES [42,43] and STM [44] experiments recently. We did not observe any sign of superconductivity in the cobalt doped multilayer FeSe thin films with the largest doping level of 8% (limited by the solubility of cobalt) down to 30 K. The different mechanism for cobalt and potassium doping behaviors of FeSe needs further experimental and theoretical studies.

As shown in Figs. 4(b) and 4(c), the spectral weight at the zone center near E_F is contributed by two holelike bands. The two band tops touch E_F in the undoped 4 UC film; with increasing cobalt doping, the holelike bands move downwards, and the hole pockets area decrease. The band topology changes significantly at M, which is shown in Figs. 4(d) and 4(e). The band structure of 3% cobalt doped FeSe film at M [Fig. 4(e2)] is very similar to that at high temperature [cut 7 in Fig. 2(d)] above the nematic transition, The nematic state is suppressed by either cobalt doping or lifted temperature, respectively. With 8% cobalt doping, an electronlike band that forms the circular Fermi pocket and a holelike band located beneath the electron band can be resolved. The band structure of 8% cobalt doped FeSe is very similar to that of 1 UC FeSe but with distinct differences. The bottom of the electron band intersect the top of the hole band in the 8% cobalt doped film at M [Fig. 4(e3)], while there is a gap between the two bands for 1 UC FeSe [Fig. 3(c1)]. At Γ, there is only one holelike band with its top 80 meV below E_F in 1 UC FeSe [Fig. 3(b1)], while two holelike bands with their tops close to E_F can be resolved in 8% cobalt doped film [Fig. 4(c3)].

The band structure evolution at Λ point is shown in Figs. 4(f) and 4(g). With about 3% cobalt doping, the Dirac

cone band dispersion in Fig. 4(g1) changes to a conventional parabolic electron band in Fig. 4(g2). Again, the band structure of 3% cobalt doped FeSe at Λ point is similar to the one at high temperature in Fig. 2(f3). Similar to iron-arsenide parent compounds, the nematic state in FeSe film can be suppressed by substitution with other 3*d* transition metals (which causes electron or hole doping). Consequently, the Dirac cone states disappear when the nematic state is suppressed.

IV. DISCUSSION AND CONCLUSION

In iron-arsenide compounds, the parent state is a collinear antiferromagnet. A theoretical study [29] found that the combination of physical symmetry and the topology of the band structure naturally stabilizes a gapless SDW ground state with Dirac nodes in undoped FeAs compound. Then, an ARPES study [31] revealed the existence of Dirac cones in the electronic structure of $BaFe_2As_2$ below the spin-density-wave temperature, which are responsible for small spots of high photoemission intensity at the Fermi level. Moreover, both electron and hole Dirac cone states are confirmed by magnetoresistance in $BaFe_2As_2$, where transverse magnetoresistance develops linearly against the magnetic field at low temperatures [32].

Similar to $BaFe_2As_2$, a recent DFT calculation [34] predicted a magnetic order named pair-checkerboard AFM as the magnetic ground state of tetragonal FeSe, which can induce Dirac cone band dispersions in FeSe. Besides, ultrafast Dirac conelike carriers were found in FeSe single crystal by electric transport measurement [33], although no static magnetic order exists in FeSe. Our ARPES data reveal that the Fermi surface of FeSe films in the nematic state is similar to $BaFe_2As_2$ in the SDW state, and similar Dirac cone band dispersions are found to be located at two small spots of high intensity. The Dirac cone band dispersions disappear when the nematic state is suppressed by increased temperature or cobalt electron doping. It is important to clarify the relation and difference of the nematic order between iron pnictides and iron chalcogenides, which can help us to understand the superconducting mechanism of iron based superconductors. Recently, different orders [18,23,34,45,46] have been proposed to explain the nematicity of FeSe, and our ARPES results provide useful information to test the existing theoretical models.

In summary, we revealed the existence of Dirac cone band dispersions in FeSe thin films thicker than 1 UC below the nematic transition temperature by photoemission spectroscopy. The Dirac cones sit at the small spots of high photoemission intensity on the Fermi surface, whose apexes are located −10 meV below Fermi energy, leading to small electron Fermi pockets. The Dirac cone structures disappear above the nematic transition temperature and barely change as a function of film thickness. Upon cobalt doping in multilayer FeSe films, the nematicity is suppressed significantly, and the Dirac cones disappear simultaneously. Our results provide useful guidelines for understanding the novel electronic structure, nematicity, and superconductivity in FeSe system.

ACKNOWLEDGMENTS

We gratefully acknowledge helpful discussions with Z. Y. Lu, Dr. L. Huang, and Dr. H. C. Xu. This work is supported by the Foundation of President of China Academy of Engineering Physics (Grant No. 201501037) and by the National Natural Science Foundation of China (Grant No. 11504341).

[1] Q.-Y. Wang, Z. Li, W.-H. Zhang, Z.-C. Zhang, J.-S. Zhang, W. Li, H. Ding, Y.-B. Ou, P. Deng, K. Chang, J. Wen, C.-L. Song, K. He, J.-F. Jia, S.-H. Ji, Y.-Y. Wang, L.-L. Wang, X. Chen, X.-C. Ma, and Q.-K. Xue, Chin. Phys. Lett. **29**, 037402 (2012).

[2] D. Liu, W. Zhang, D. Mou, J. He, Y. B. Ou, Q. Y. Wang, Z. Li, L. Wang, L. Zhao, S. He, Y. Peng, X. Liu, C. Chen, L. Yu, G. Liu, X. Dong, J. Zhang, C. Chen, Z. Xu, J. Hu *et al.*, Nat. Commun. **3**, 931 (2012).

[3] S. He, J. He, W. Zhang, L. Zhao, D. Liu, X. Liu, D. Mou, Y.-B. Ou, Q.-Y. Wang, Z. Li, L. Wang, Y. Peng, Y. Liu, C. Chen, L. Yu, G. Liu, X. Dong, J. Zhang, C. Chen, Z. Xu *et al.*, Nat. Mater. **12**, 605 (2013).

[4] S. Y. Tan, Y. Zhang, M. Xia, Z. R. Ye, F. Chen, X. Xie, R. Peng, D. F. Xu, Q. Fan, H. C. Xu, J. Juan, T. Zhang, X. C. Lai, T. Xiang, J. P. Hu, B. P. Xie, and D. L. Feng, Nat. Mater. **12**, 634 (2013).

[5] J. J. Lee, F. T. Schmitt, R. G. Moore, S. Johnston, Y. T. Cui, W. Li, M. Yi, Z. K. Liu, M. Hashimoto, Y. Zhang, D. H. Lu, T. P. Devereaux, D. H. Lee, and Z. X. Shen, Nature (London) **515**, 245 (2014).

[6] R. Peng, X. P. Shen, X. Xie, H. C. Xu, S. Y. Tan, M. Xia, T. Zhang, H. Y. Cao, X. G. Gong, J. P. Hu, B. P. Xie, and D. L. Feng, Phys. Rev. Lett. **112**, 107001 (2014).

[7] R. Peng, H. C. Xu, S. Y. Tan, H. Y. Cao, M. Xia, X. P. Shen, Z. C. Huang, C. H. Wen, Q. Song, T. Zhang, B. P. Xie, X. G. Gong, and D. L. Feng, Nat. Commun. **5**, 5044 (2014).

[8] W. Zhang, Y. Sun, J. Zhang, F. Li, M. Guo, Y. Zhao, H. Zhang, J. Peng, Y. Xing, H. Wang, T. Fujita, A. Hirata, Z. Li, H. Ding, C. Tang, M. Wang, Q. Wang, K. He, S. Ji, X. Chen *et al.*, Chin. Phys. Lett. **31**, 017401 (2013).

[9] J. F. Ge, Z. L. Liu, C. Liu, C. L. Gao, D. Qian, Q. K. Xue, Y. Liu, and J. F. Jia, Nat. Mater. **14**, 285 (2014).

[10] F. C. Hsu, J. Y. Luo, K. W. Yeh, T. K. Chen, T. W. Huang, P. M. Wu, Y. C. Lee, Y. L. Huang, Y. Y. Chu, D. C. Yan, and M. K. Wu, Proc. Natl. Acad. Sci. USA **105**, 14262 (2008).

[11] K. Nakayama, Y. Miyata, G. N. Phan, T. Sato, Y. Tanabe, T. Urata, K. Tanigaki, and T. Takahashi, Phys. Rev. Lett. **113**, 237001 (2014).

[12] S. H. Baek, D. V. Efremov, J. M. Ok, J. S. Kim, J. van den Brink, and B. Büchner, Nat. Mater. **14**, 210 (2014).

[13] T. Shimojima, Y. Suzuki, T. Sonobe, A. Nakamura, M. Sakano, J. Omachi, K. Yoshioka, M. Kuwata-Gonokami, K. Ono, H. Kumigashira, A. E. Böhmer, F. Hardy, T. Wolf, C. Meingast, H. v. Löhneysen, H. Ikeda, and K. Ishizaka, Phys. Rev. B **90**, 121111(R) (2014).

[14] A. E. Böhmer, T. Arai, F. Hardy, T. Hattori, T. Iye, T. Wolf, H. v. Löhneysen, K. Ishida, and C. Meingast, Phys. Rev. Lett. **114**, 027001 (2015).

[15] A. V. Chubukov, R. M. Fernandes, and J. Schmalian, Phys. Rev. B **91**, 201105(R) (2015).
[16] S. Mukherjee, A. Kreisel, P. J. Hirschfeld, and B. M. Andersen, Phys. Rev. Lett. **115**, 026402 (2015).
[17] M. C. Rahn, R. A. Ewings, S. J. Sedlmaier, S. J. Clarke, and A. T. Boothroyd, Phys. Rev. B **91**, 180501(R) (2015).
[18] F. Wang, S. A. Kivelson, and D.-H. Lee, Nat. Phys. **11**, 959 (2015).
[19] M. D. Watson, T. K. Kim, A. A. Haghighirad, N. R. Davies, A. McCollam, A. Narayanan, S. F. Blake, Y. L. Chen, S. Ghannadzadeh, A. J. Schofield, M. Hoesch, C. Meingast, T. Wolf, and A. I. Coldea, Phys. Rev. B **91**, 155106 (2015).
[20] P. Zhang, T. Qian, P. Richard, X. P. Wang, H. Miao, B. Q. Lv, B. B. Fu, T. Wolf, C. Meingast, X. X. Wu, Z. Q. Wang, J. P. Hu, and H. Ding, Phys. Rev. B **91**, 214503 (2015).
[21] Q. Wang, Y. Shen, B. Pan, Y. Hao, M. Ma, F. Zhou, P. Steffens, K. Schmalzl, T. R. Forrest, M. Abdel-Hafiez, X. Chen, D. A. Chareev, A. N. Vasiliev, P. Bourges, Y. Sidis, H. Cao, and J. Zhao, Nat. Mater. **15**, 159 (2015).
[22] Y. Zhang, M. Yi, Z.-K. Liu, W. Li, J. J. Lee, R. G. Moore, M. Hashimoto, N. Masamichi, H. Eisaki, S.-K. Mo, Z. Hussain, T. P. Devereaux, Z.-X. Shen, and D. H. Lu, arXiv:1503.01556.
[23] S. Onari, Y. Yamakawa, and H. Kontani, arXiv:1509.01172.
[24] S. Y. Zhou, G. H. Gweon, J. Graf, A. V. Fedorov, C. D. Spataru, R. D. Diehl, Y. Kopelevich, D. H. Lee, S. G. Louie, and A. Lanzara, Nat. Phys. **2**, 595 (2006).
[25] M. Z. Hasan and C. L. Kane, Rev. Mod. Phys. **82**, 3045 (2010).
[26] X.-L. Qi and S.-C. Zhang, Rev. Mod. Phys. **83**, 1057 (2011).
[27] X. Wan, A. M. Turner, A. Vishwanath, and S. Y. Savrasov, Phys. Rev. B **83**, 205101 (2011).
[28] G. Xu, H. Weng, Z. Wang, X. Dai, and Z. Fang, Phys. Rev. Lett. **107**, 186806 (2011).
[29] Y. Ran, F. Wang, H. Zhai, A. Vishwanath, and D.-H. Lee, Phys. Rev. B **79**, 014505 (2009).
[30] N. Harrison and S. E. Sebastian, Phys. Rev. B **80**, 224512 (2009).
[31] P. Richard, K. Nakayama, T. Sato, M. Neupane, Y. M. Xu, J. H. Bowen, G. F. Chen, J. L. Luo, N. L. Wang, X. Dai, Z. Fang, H. Ding, and T. Takahashi, Phys. Rev. Lett. **104**, 137001 (2010).
[32] K. K. Huynh, Y. Tanabe, and K. Tanigaki, Phys. Rev. Lett. **106**, 217004 (2011).
[33] K. K. Huynh, Y. Tanabe, T. Urata, H. Oguro, S. Heguri, K. Watanabe, and K. Tanigaki, Phys. Rev. B **90**, 144516 (2014).
[34] H.-Y. Cao, S. Chen, H. Xiang, and X.-G. Gong, Phys. Rev. B **91**, 020504 (2015).
[35] L. X. Yang, Y. Zhang, H. W. Ou, J. F. Zhao, D. W. Shen, B. Zhou, J. Wei, F. Chen, M. Xu, C. He, Y. Chen, Z. D. Wang, X. F. Wang, T. Wu, G. Wu, X. H. Chen, M. Arita, K. Shimada, M. Taniguchi, Z. Y. Lu *et al.*, Phys. Rev. Lett. **102**, 107002 (2009).
[36] C. He, Y. Zhang, B. P. Xie, X. F. Wang, L. X. Yang, B. Zhou, F. Chen, M. Arita, K. Shimada, H. Namatame, M. Taniguchi, X. H. Chen, J. P. Hu, and D. L. Feng, Phys. Rev. Lett. **105**, 117002 (2010).
[37] S. V. Borisenko, D. V. Evtushinsky, Z.-H. Liu, I. Morozov, R. Kappenberger, S.Wurmeh, B. Büchner, A. N. Yaresko, T. K. Kim, M. Hoesch, T. Wolf, and N. D. Zhigadlo, Nat. Phys. (2015).
[38] W. Li, Y. Zhang, J. J. Lee, H. Ding, M. Yi, Z. Li, P. Deng, K. Chang, S.-K. Mo, M. Hashimoto, D. H. Lu, X. Chen, R. G. Moore, Q.-K. Xue, and Z.-X. Shen, arXiv:1509.01892.
[39] M. Matusiak, Z. Bukowski, and J. Karpinski, Phys. Rev. B **83**, 224505 (2011).
[40] H.-H. Kuo, J.-H. Chu, S. C. Riggs, L. Yu, P. L. McMahon, K. De Greve, Y. Yamamoto, J. G. Analytis, and I. R. Fisher, Phys. Rev. B **84**, 054540 (2011).
[41] A. Tamai, A. Y. Ganin, E. Rozbicki, J. Bacsa, W. Meevasana, P. D. C. King, M. Caffio, R. Schaub, S. Margadonna, K. Prassides, M. J. Rosseinsky, and F. Baumberger, Phys. Rev. Lett. **104**, 097002 (2010).
[42] Y. Miyata, K. Nakayama, K. Sugawara, T. Sato, and T. Takahashi, Nat. Mater. **14**, 775 (2015).
[43] C. H. P. Wen, H. C. Xu, C. Chen, Z. C. Huang, Y. J. Pu, Q. Song, B. P. Xie, M. Abdel-Hafiez, D. A. Chareev, A. N. Vasiliev, R. Peng, and D. L. Feng, arXiv:1508.05848.
[44] Q. Fan, W. H. Zhang, X. Liu, Y. J. Yan, M. Q. Ren, R. Peng, H. C. Xu, B. P. Xie, J. P. Hu, T. Zhang, and D. L. Feng, Nat. Phys. **11**, 946 (2015).
[45] R. Yu and Q. Si, Phys. Rev. Lett. **115**, 116401 (2015).
[46] Y. Liang, X.-X. Wu, and J.-P. Hu, Chin. Phys. Lett. **32**, 117402 (2015).